

Discovery of First-in-Class Small Molecule Inhibitors of Lymphocyte Activation Gene 3 (LAG-3)

Somaya A. Abdel-Rahman, Ashfaq Ur Rehman, and Moustafa T. Gabr*

Cite This: *ACS Med. Chem. Lett.* 2023, 14, 629–635

Read Online

ACCESS |



Metrics & More



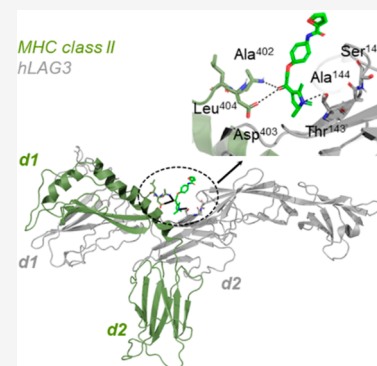
Article Recommendations



Supporting Information

ABSTRACT: Lymphocyte activation gene 3 (LAG-3) is a negative immune checkpoint that plays a key role in downregulating the immune response to cancer. Inhibition of LAG-3 interactions allows T cells to regain cytotoxic activity and reduce the immunosuppressive function of regulating T cells. We utilized a combination approach of focused screening and “SAR by catalog” to identify small molecules that function as dual inhibitors of the interactions of LAG-3 with major histocompatibility complex (MHC) class II and fibrinogen-like protein 1 (FGL1). Our top hit compound inhibited both LAG-3/MHCII and LAG-3/FGL1 interactions in biochemical binding assays with IC_{50} values of 4.21 ± 0.84 and $6.52 \pm 0.47 \mu\text{M}$, respectively. Moreover, we have demonstrated the ability of our top hit compound to block LAG-3 interactions in cell-based assays. This work will pave the way for future drug discovery efforts aiming at the development of LAG-3-based small molecules for cancer immunotherapy.

KEYWORDS: Checkpoints, LAG-3, cancer immunotherapy, drug discovery, immunomodulators



Advancements in immune checkpoint blockade (ICB) therapy have resulted in remarkable clinical success in the treatment of several types of cancers, leading to improved survival for a subset of patients.^{1–3} This is primarily due to the use of monoclonal antibodies (mAbs) that target immune checkpoints, such as programmed cell death protein 1 (PD-1) and cytotoxic T-lymphocyte associated protein 4 (CTLA-4).^{4,5} However, the majority of cancer patients do not respond effectively to ICB, either due to primary or acquired resistance.^{6–9} This can be caused by both intrinsic factors within cancer cells and extrinsic factors in the tumor microenvironment (TME). Consequently, recent research efforts have focused on targeting alternative immune checkpoints, such as lymphocyte activation gene 3 (LAG-3), T-cell immunoglobulin mucin-3 (TIM-3), and V-domain immunoglobulin suppressor of T-cell activation (VISTA), to increase the number of patients who can benefit from ICB.^{6–9}

LAG-3, a cell surface inhibitory receptor and an established target for cancer immunotherapy, is expressed on activated T cells, natural killer (NK) cells, B cells, and plasmacytoid dendritic cells.^{10–13} Similarly to PD-1 and CTLA-4, LAG-3 is not expressed on naive T cells. However, the expression of LAG-3 is induced on CD4⁺ and CD8⁺ T cells upon antigen stimulation.^{14,15} LAG-3 synergizes with other inhibitory checkpoints (e.g., PD-1 and CTLA-4) to improve the inhibitory activity of regulatory T cells, leading to antigen-presenting cells (APCs)-induced immune tolerance.¹⁶ LAG-3 positive T cells bind LAG-3 ligands (major histocompatibility complex (MHC) class II and Fibrinogen-like protein 1 (FGL1)), which inhibits activation and cytokine secretion via

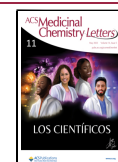
indirectly blocking T cell receptor (TCR) signaling.^{10–13} Notably, the interaction between LAG-3 and MHCII, the canonical ligand of LAG-3, triggers MHCII signal transduction in dendritic cells, activating phospholipase C $\gamma 2$, p72syk, PI3K/AKT, p42/44, and p38 protein kinase.¹⁷ FGL1, a liver-secreted protein, has been recently identified as a major LAG-3 functional ligand that inhibits antigen-specific T-cell activation.¹⁸ Blockade of LAG-3/FGL1 interaction by mAbs is an established therapeutic strategy to enhance tumor immunity in preclinical and clinical studies.^{18,19}

LAG-3 is highly expressed on tumor-infiltrating lymphocytes (TILs) of various solid tumors, including colon cancer, nonsmall cell lung cancer (NSCLC), head and neck cell cancer, and pancreatic cancer.^{20–23} LAG-3 and PD-1 suppress T cell stimulation through different signaling pathways, thus, both function synergistically in mediating T-cell exhaustion. In this context, numerous reports have revealed that coblockade of PD-1 and LAG3 expressed on CD8⁺ and CD4⁺ TILs exhibited enhanced antitumor responses in preclinical animal models of ovarian cancer, colon adenocarcinoma, and melanoma.^{24–26} Notably, a clinical trial named RELATIV-ITY-047 revealed that the combination of anti-LAG-3 and anti-

Received: February 14, 2023

Accepted: April 6, 2023

Published: April 11, 2023



PD-1 mAbs produced a median progression-free survival of 10.1 months in patients with metastatic melanoma, compared to only 4.6 months using anti-PD-1 mAb alone.²⁷ This combination therapy, known as relatlimab (anti-LAG-3) and nivolumab (anti-PD-1), has received approval from the U.S. Food and Drug Administration (FDA) in 2022 for use in metastatic melanoma patients.²⁷

Given the established therapeutic potential in targeting LAG-3 interactions to improve the outcome of ICB,^{24–27} numerous agents are currently being evaluated in preclinical and clinical studies as combination therapies for several solid tumors. However, the inhibition of LAG-3 interactions is currently restricted to mAbs, and there are no small molecules in existence that function as LAG-3 inhibitors. In general, there are disadvantages to using mAbs as a therapeutic modality, such as suboptimal tumor penetration, high manufacturing costs, and potential immunogenicity.^{28–31} Importantly, mAbs generally possess prolonged half-lives, potentially resulting in long-term on-target mediated immune-related adverse events (irAEs).^{32,33} In comparison to mAbs, small molecules have oral bioavailability and enhanced tumor penetration.^{34,35} Remarkably, small molecules are more amenable to pharmacokinetic optimization, which allows adopting flexible dosage regimens that may enable avoiding irAEs associated with mAbs. Therefore, the discovery of small molecule LAG-3 inhibitors would enable the development of combination treatments that have the potential for clinical translation as efficient immunotherapies for multiple solid tumors.

Building on our previously reported work focused on the discovery of small molecule immune checkpoint inhibitors,³⁶ we initiated a screening workflow to identify small molecule LAG-3 inhibitors (Figure 1). A recent report revealed that

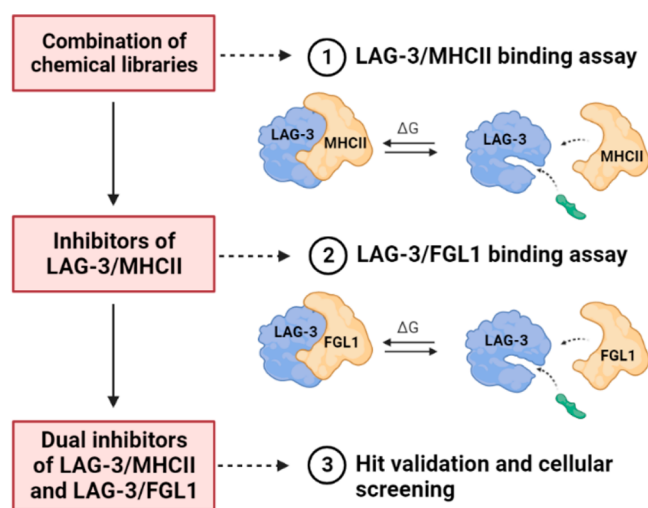


Figure 1. Schematic representation of our screening workflow to identify small molecule LAG-3 inhibitors.

binding of LAG-3 to stable pMHCII but not to FGL1 induced T cell suppression *in vitro*.³⁷ However, the FDA-approved LAG-3 mAb, relatlimab, has demonstrated the ability to block both LAG-3/MHCII and LAG-3/FGL1 interactions.³⁸ Moreover, FGL1 has been reported to trigger cell surface LAG-3 to transmit signals for T cell suppression.¹⁸ Thus, the focus of our screening strategy is to identify small molecule dual inhibitors of LAG-3/MHCII and LAG-3/FGL1 interactions. As shown in Figure 1, our strategy is based on screening a diversified

chemical library for the ability to block LAG-3/MHCII inhibition, followed by screening validated inhibitors of LAG-3/MHCII for the ability to inhibit LAG-3/FGL1 interaction.

We established a chemical library (~3000 compounds) with diversified chemical structures. Our library entailed compounds from the NCI Diversity Set VII, FDA-approved drugs, bioactive compounds from APExBIO, Discovery Diversity Set from Enamine, and CORE library stock from ChemBridge. Notably, the characteristics of this library comply with Lipinski's rule of Five, a valuable parameter for evaluating drug-likeness of small molecules based on their physicochemical properties.³⁹ Moreover, we removed promiscuous compounds from our diversified chemical library using the PAINS (Pan-Assay Interference Compounds) filter.⁴⁰ Initially, we subjected our chemical library to single-dose (50 μM) screening using homogeneous time-resolved fluorescence (HTRF) LAG-3/MHCII biochemical binding assay from Cisbio. This is a time-Resolved fluorescence resonance energy transfer (TR-FRET) immunoassay that employs tagging LAG-3 with europium cryptate as a fluorescent donor and MHCII with a fluorescence acceptor. When the two proteins interact, the donor molecule is brought within proximity of the acceptor molecule. Excitation of the donor will result in signal generation proportional to the binding of proteins. Agents that block the interaction between both proteins result in attenuated TR-FRET signal. Hits were identified by the ability to decrease the TR-FRET signal by more than 5 standard deviations (5 SD) lower than the total mean. We further screened the hits for the ability to block LAG-3/FGL1 interaction using TR-FRET assay from BPS Bioscience. Notably, the utility of both LAG-3/MHCII and LAG-3/FGL1 TR-FRET assays for HTS has been demonstrated with mean Z' factors of 0.76 ± 0.04 and 0.68 ± 0.02 , respectively, revealing high-quality assay for HTS. Z' factor corresponds to the ratio of data signal variability (standard deviation) to dynamic range (i.e., change in TR-FRET signal for positive and negative controls). SA-15 (Figure 2a) exhibited remarkable attenuation of the TR-FRET signal (>90%) of LAG-3/MHCII in comparison to the identified hits. Dose-dependent TR-FRET screening was conducted for SA-15, which revealed a half maximal inhibitory concentration (IC_{50}) value of $14.81 \pm 0.92 \mu\text{M}$ (Figure 2b). Remarkably, SA-15 revealed an IC_{50} value of $16.67 \pm 1.42 \mu\text{M}$ for the inhibition of LAG-3/FGL1 in TR-FRET assay (Figure S1) and $18.51 \pm 1.79 \mu\text{M}$ in LAG-3/FGL1 ELISA (Figure S2).

Despite the emergence of LAG-3/MHCII interaction as a target for next-generation immunotherapies, we have little information describing the binding mechanism of LAG-3 and MHCII or potential binding mechanisms of small molecules inhibiting LAG-3/MHCII signaling. To elucidate the potential binding mode of SA-15 at the LAG-3/MHCII interface, we performed molecular dynamics (MD) simulation via AMBER v2018. Our study has revealed that both proteins (LAG-3 and MHCII) are associated with each other until SA-15 binds to the interface leading to inducing conformational rotation in both domains (d1 & d2) of MHCII. This rotation further brings both domains of LAG-3 closer (decreases the distance between d1 and d2). Our results also confirm that binding of SA-15 to a novel cryptic site (interface) brings this conformational dynamic in both proteins and most probably, it is possible that the complex of LAG-3 with MHCII will be

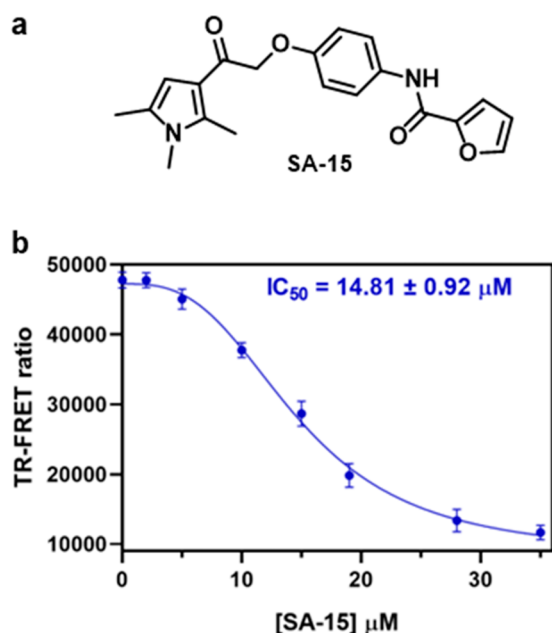


Figure 2. (a) Chemical structure of SA-15. (b) Dose–response curve of SA-15 in TR-FRET assay of LAG-3/MHCII assay. Error bars represent standard deviation ($n = 3$).

dissociated when the compound resides longer enough in the interface.

In detail, we have simulated fully solvated atomistic models of the LAG-3/MHCII conformation in the presence of SA-15 for a total of 1.0 μ s, i.e., 0.5 μ s for each run. The simulated complex includes SA-15, LAG-3 (d1–d4), and MHCII (d1–d2). The deviation of backbone atoms was examined by root-mean-square-deviation (RMSD). The core-RMSD of both runs relative to the original structures illustrates that 500 ns of MD simulation time is adequate to attain equilibration at 310 K. The average core-RMSD results of both runs share similarity except for the initial 100 ns and indicate the stability of the overall system in an explicit solvent condition (Figure 3a). Moreover, our dynamics results, i.e., principal component analysis (PCA), revealed a dramatic conformational shift in both LAG-3 and MHCII proteins after the trajectory reached 100 ns MD time (see PCA movie in the Supporting Information). This observation indicates that at the initial 100 ns MD time, both proteins were associated with each other, but after 100 ns MD time, compound SA-15 bound to the interface of both proteins. This binding further induces conformational changes in both d1 and d2 of LAG-3 and MHCII to rotate (Figure 2b).

To understand the degree of fluctuation of individual residues, we analyzed the root-mean-square fluctuations (RMSF), which provide information about the degree of flexibility of each residue. The minimal energy structural

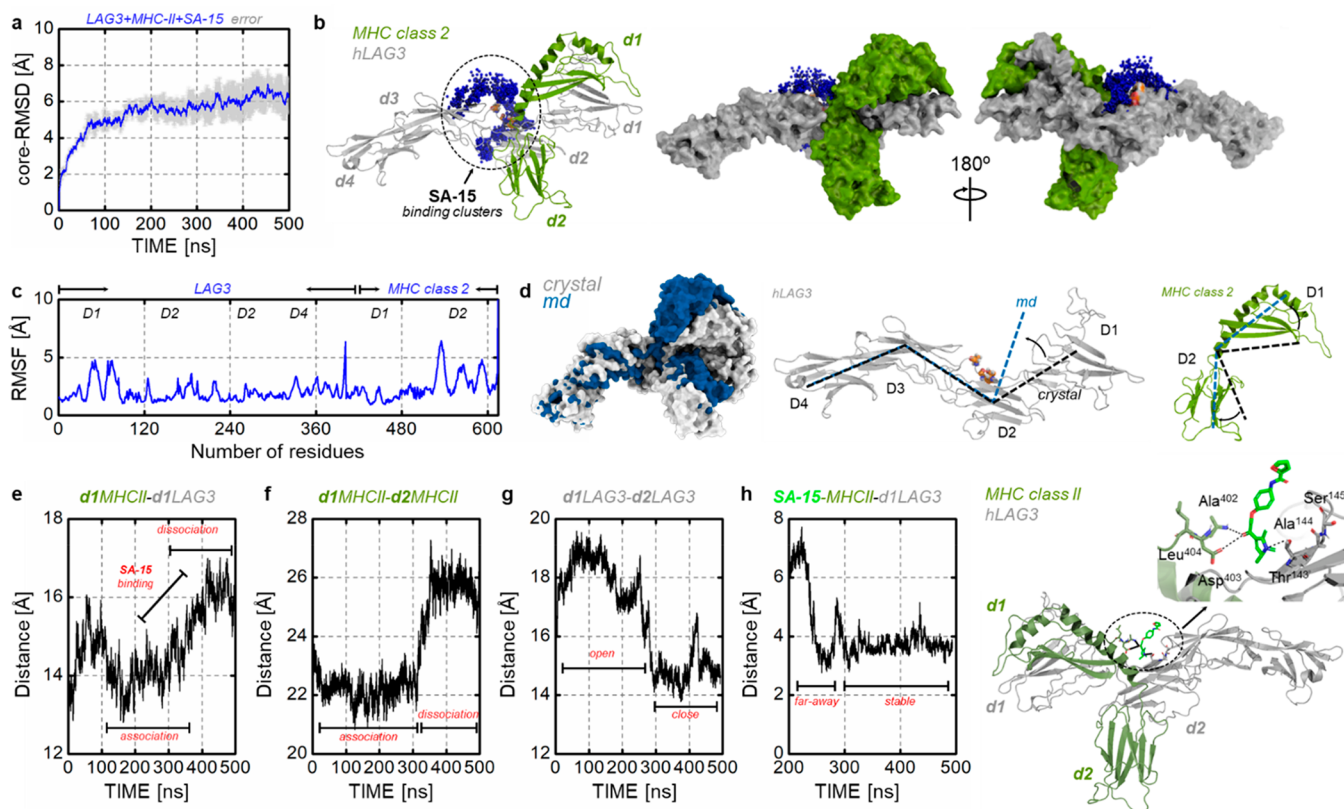
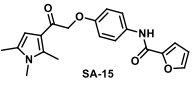
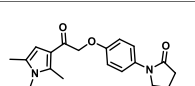
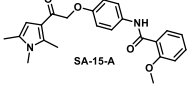
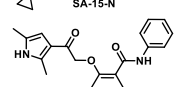
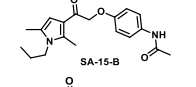
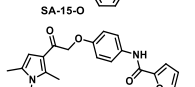
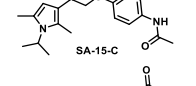
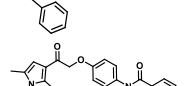
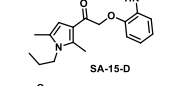
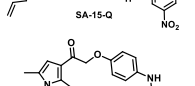
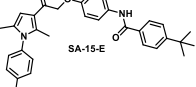
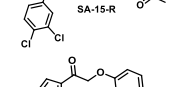
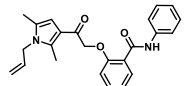
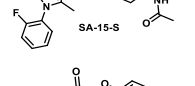
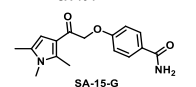
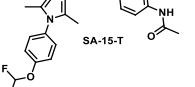
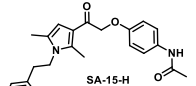
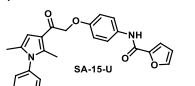
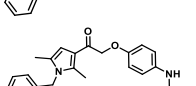
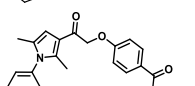
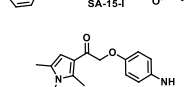
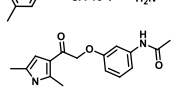

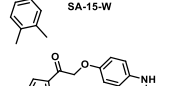
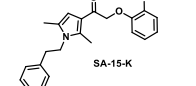
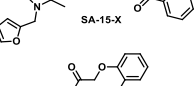
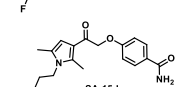


Figure 3. Illustration of the dynamics of LAG-3/MHCII in complex with compound SA-15. (a) Core-RMSD graph, the blue color indicates the average core-RMSD of the system, while the gray transparency represents the error. (b) Cluster for compound SA-15 which binds to the LAG-3/MHCII interface; the structure is displayed in both the cartoon and surface. (c) Representation of the residues fluctuation index (RMSF). (d) Illustration of the superposed (only aligning the LAG-3) to show the conformational change (indicated by the dotted lines) of our simulated model (md) and the crystal structure. (e–h) Demonstration of the CA-distance analysis for LAG-3 and MHCII domains and the CA-distance between compound SA-15 and the cryptic site residues. The interaction of compound SA-15 has been shown in cartonic representation.

Table 1. SA-15 Structural Analogues and their LAG-3 Inhibitory Profiles Based on LAG-3/MHCII and LAG-3/FGL1 TR-FRET Assays^a

Compound	IC ₅₀ (μM) of LAG-3/MHCII	IC ₅₀ (μM) of LAG-3/FGL1	Compound	IC ₅₀ (μM) of LAG-3/MHCII	IC ₅₀ (μM) of LAG-3/FGL1
	14.81 ± 0.92	16.67 ± 1.42		17.24 ± 1.34	20.42 ± 1.03
	25.67 ± 1.34	35.39 ± 2.41		>50	>50
	>50	>50		4.21 ± 0.84	6.52 ± 0.47
	>50	>50		>50	>50
	>50	>50		11.22 ± 1.93	10.32 ± 0.38
	19.32 ± 2.12	18.24 ± 1.34		21.34 ± 1.43	29.45 ± 2.18
	>50	>50		12.42 ± 1.24	16.53 ± 1.35
	>50	>50		8.36 ± 0.31	13.74 ± 1.12
	23.42 ± 1.34	28.49 ± 3.42		26.95 ± 1.93	29.42 ± 2.15
	18.32 ± 0.46	20.45 ± 1.74		31.35 ± 2.48	25.48 ± 1.39
	28.45 ± 2.24	21.35 ± 1.54		9.38 ± 0.36	9.94 ± 1.03
	28.45 ± 1.46	32.69 ± 1.93		18.35 ± 1.32	14.25 ± 0.83
	18.34 ± 1.42	22.42 ± 0.94		20.42 ± 0.39	28.73 ± 1.48
	>50	>50			

^aIC₅₀ values (μM) are presented ± standard deviation (*n* = 3).

coordinates for both states were extracted from PCA. The coordinates of both were first aligned, and then the average structure for each state was used as a reference to calculate the

residue fluctuation. The results show a dramatic fluctuation, particularly in the d1 of LAG-3 and in the d1 and d2 of MHCII proteins (Figure 3c). Moreover, we have compared the

crystallographic and the average trajectory coordinates by aligning solely the core domains of LAG-3 protein, we have found that our simulated model showed different conformations of MHCII protein, where both of their domains change the conformation from V-shape to more open shape (Figure 3d). In addition, the angle between them is increased than the crystal upon binding of SA-15 to the interface. The binding cluster for SA-15 has been extracted from the overall trajectory (Figure 3b), and we have found that the SA-15 resides in this cryptic site for almost 90% of the total MD time.

Moreover, we have analyzed the CA-distance between d1 and d1 of both LAG-3 and MHCII in order to confirm the induced conformational changes induced by SA-15 that results in the dissociation of both complexes. The CA-distance between d1 of LAG-3 and d1 of MHCII revealed that both complexes were tightly associated with each other around 250 ns MD time (Figure 3e), but a gradual increase in CA-distance has been observed, which indicates that d1 of LAG-3 moved away from d1 of MHCII. Moreover, we have analyzed the CA-distance between d1 and d2 of solely MHC II to confirm the conformational change in their domain, which changes from a V-shape to a more open conformation. The results revealed that a sudden change was observed after 300 ns MD time, which indicates that both domains moved away from each other, and in this way, both domains adopted a more open conformation (Figure 3f). Moreover, the CA-distance between d1 and d2 of LAG-3 revealed that initially the CA-distance between them was $\sim 18\text{--}19$ Å, but gradually, the CA-distance between them decreased, which indicates that both the domains are close to each other (Figure 3g). Based on these results, SA-15 binds to the interface of both proteins and resides long enough in the interface, which results in a dramatic conformational change in both the d1 and d2 of LAG-3 and MHCII. We have analyzed the CA-distance between SA-15 and the bonded residues, including residue Thr143, Ala144, Ser145, Ala402, Asp403 and Leu404 (Figure 3h, right panel). We have excluded the initial 100 ns, where the SA-15 bound at different sites (none of them at the interface) for some picoseconds (ps). Initially, the results indicate an increase in CA-distance measure and then oscillated until 500 ns MD time; this slight high distance is due to the rotation of the unbound moiety of SA-15, attempting to accommodate in the binding site (Figure 3h). Our dynamics results indicate that the binding of compound SA-15 to the complex of both LAG-3 and MHCII brings about dramatic conformational changes in d1 and d2 of both proteins. This dramatic conformational change further creates a cryptic site to accommodate compound SA-15.

Structure–activity relationship (SAR) by catalog is an established approach to investigate the impact of structural variations in identified hits from screening platforms on the desired biological activity.^{41–43} This approach relies on purchasing structural analogs of the desired hit compounds from commercial sources. Therefore, we procured 26 structural analogs of SA-15 from Enamine and evaluated the ability of these structural analogs to inhibit both LAG-3/MHCII and LAG-3/FGL1 interactions (Table 1). The top hit compound from this approach (SA-15-P, Table 1) possessed IC_{50} values of 4.21 ± 0.84 and 6.52 ± 0.47 μM for LAG-3/MHCII and LAG-3/FGL1 interactions, respectively. In comparison to SA-15, SA-15-P incorporates an additional N-phenethyl substituent (Table 1). Notably, the replacement of the furyl ring in SA-15 with various substituted phenyl moieties resulted in a

reduction in the LAG-3 inhibitory profile (e.g., SA-15-A, SA-15-E, and SA-15-F). Moreover, the removal of the furyl ring from SA-15 abolished the LAG-3 inhibitory profile of the screened structural analogs (e.g., SA-15-B, SA-15-C, SA-15-D, SA-15-G, and SA-15-M). Such effect was partially alleviated upon substitution of the pyrrole core with various aromatic moieties (e.g., SA15-H, SA15-I, SA-15-J, SA-15-K, SA-15-L, SA-15-R, SA-15-S, SA-15-T, SA-15-V, and SA-15-W). Remarkably, our study has revealed that the substitution of the pyrrole core with alicyclic moieties holds promise for future development of compounds with balanced inhibitory profiles for LAG-3/MHCII and LAG-3/FGL1 interactions (e.g., SA-15-N and SA-15-Y).

We further evaluated the ability of our top hit compound, SA-15-P, to block LAG-3/MHCII interaction in a cell-based assay. For this, we utilized a bioluminescent cell-based assay from Promega that evaluates the ability of agents to block LAG-3/MHCII interaction. The bioassay consists of two cell lines, MHCII-positive human cell line and NanoLuc (NL) luciferase reporter/Jurkat LAG-3 cells. When cocultured, the LAG-3 inhibits TCR pathway-activated luminescence. The addition of anti-LAG-3 antibody blocks LAG-3 binding to MHCII, resulting in full TCR pathway activation, which can be detected in a dose-dependent manner by the addition of Bio-Glo Reagent and quantitation with a luminometer. As shown in Figure 4, SA-15-P resulted in dose-dependent enhancement

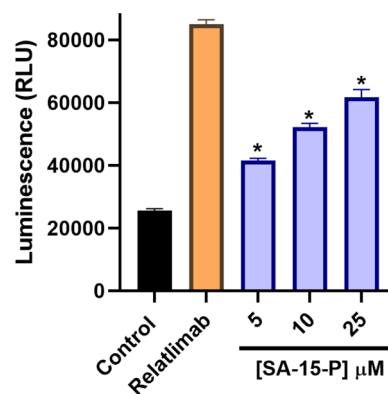


Figure 4. LAG-3/MHCII blockade assay from Promega. Measured luminescence upon coculturing LAG-3 effectors and MHCII APC cells in the absence and the presence of relatimab (5 nM) and varying concentrations of SA-15-P. Error bars represent standard deviation ($n = 3$) (* $p < 0.01$ relative to untreated control).

in the luminescence signal of the Promega LAG-3/MHCII blockade cellular assay revealing the ability to inhibit the interaction between both proteins expressed on cell surfaces. The IC_{50} value of SA-15-P in the Promega LAG-3/MHCII assay (6.95 ± 1.05 μM) was in close agreement with the IC_{50} value of SA-15-P in the TR-FRET LAG-3/MHCII assay (4.21 ± 0.84 μM). In addition, we utilized a cell-based ligand–receptor blocking assay to verify the ability of SA-15-P to block the binding of a fixed concentration of FGL1-hFc to CHO-K1/LAG-3 stable cell line (Figure S3).

In summary, we have implemented a screening workflow that enables the identification of first-in-class small molecule LAG-3 inhibitors that block both LAG-3/MHCII and LAG-3/FGL1 interactions. Our combination approach of focused screening and “SAR by catalog” resulted in the identification of SA-15-P with IC_{50} values of 4.21 ± 0.84 and 6.52 ± 0.47 μM

for LAG-3/MHCII and LAG-3/FGL1 interactions, respectively. Preliminary *in vitro* evaluation of SA-15-P revealed its ability to block LAG-3-mediated interactions in coculture cellular assays. Further structural modifications of SA-15-P will set the stage for further preclinical evaluation of the optimized small molecule LAG-3 inhibitors in animal models for immuno-oncology.

■ ASSOCIATED CONTENT

SI Supporting Information

The Supporting Information is available free of charge at <https://pubs.acs.org/doi/10.1021/acsmchemlett.3c00054>.

Experimental procedures, cellular assays, and computational studies (PDF)

Conformational shift in both LAG-3 and MHCII proteins after the trajectory reached 100 ns MD time (AVI)

■ AUTHOR INFORMATION

Corresponding Author

Moustafa T. Gabr – Department of Radiology, Molecular Imaging Innovations Institute (MI3), Weill Cornell Medicine, New York, New York 10065, United States; orcid.org/0000-0001-9074-3331; Email: mog4005@med.cornell.edu

Authors

Somaya A. Abdel-Rahman – Department of Radiology, Molecular Imaging Innovations Institute (MI3), Weill Cornell Medicine, New York, New York 10065, United States; Department of Medicinal Chemistry, Faculty of Pharmacy, Mansoura University, Mansoura 35516, Egypt

Ashfaq Ur Rehman – Department of Molecular Biology and Biochemistry, University of California, Irvine, Irvine, California 92697, United States

Complete contact information is available at: <https://pubs.acs.org/10.1021/acsmchemlett.3c00054>

Author Contributions

The manuscript was written through contributions of all authors. All authors have given approval to the final version of the manuscript.

Notes

The authors declare no competing financial interest.

■ ABBREVIATIONS

LAG-3, Lymphocyte activation gene 3; ICB, immune checkpoint blockade; mAbs, monoclonal antibodies; PD-1, programmed cell death protein 1; CTLA-4, cytotoxic T-lymphocyte associated protein 4; TME, tumor microenvironment; TIM-3, T-cell immunoglobulin mucin-3; VISTA, V-domain immunoglobulin suppressor of T-cell activation; TCR, T cell receptor; NK cells, natural killer cells; APCs, antigen-presenting cells; TILs, tumor-infiltrating lymphocytes; NSCLC, nonsmall cell lung cancer; FDA, Food and Drug Administration; irAEs, immune-related adverse events; MD, molecular dynamics; RMSD, root-mean-square-deviation; RMSF, root-mean-square fluctuations; PCA, principal component analysis; SAR, structure–activity relationship; MHC, major histocompatibility complex; FGL1, Fibrinogen-like protein 1; HTRF, homogeneous time-resolved fluorescence; FRET, fluorescence resonance energy transfer

■ REFERENCES

- Huang, A. C.; Zappasodi, R. A decade of checkpoint blockade immunotherapy in melanoma: understanding the molecular basis for immune sensitivity and resistance. *Nat. Immunol.* **2022**, *23* (5), 660–670.
- Zhang, Y.; Zhang, Z. The history and advances in cancer immunotherapy: understanding the characteristics of tumor-infiltrating immune cells and their therapeutic implications. *Cell. Mol. Immunol.* **2020**, *17*, 807–821.
- Shiravand, Y.; Khodadadi, F.; Kashani, S. M.; Hosseini-Fard, S. R.; Hosseini, S.; Sadeghirad, H.; Ladwa, R.; O'Byrne, K.; Kulasinghe, A. Immune checkpoint inhibitors in cancer therapy. *Curr. Oncol.* **2022**, *29* (5), 3044–3060.
- Seidel, J. A.; Otsuka, A.; Kabashima, K. Anti-PD-1 and anti-CTLA-4 therapies in cancer: Mechanism of action, efficacy, and limitations. *Front Oncol.* **2018**, *8*, 86.
- Chae, Y. K.; Arya, A.; Iams, W.; Cruz, M. R.; Chandra, S.; Choi, J.; Giles, F. Current landscape and future of dual anti-CTLA4 and PD-1/PD-L1 blockade immunotherapy in cancer; lessons learned from clinical trials with melanoma and non-small cell lung cancer (NSCLC). *J. Immunother. Cancer* **2018**, *6* (1), 39.
- Schoenfeld, A. J.; Hellmann, M. D. Acquired Resistance to Immune Checkpoint Inhibitors. *Cancer Cell* **2020**, *37* (4), 443–455.
- Jenkins, R. W.; Barbie, D. A.; Flaherty, K. T. Mechanisms of resistance to immune checkpoint inhibitors. *Br. J. Cancer* **2018**, *118* (1), 9–16.
- Barrueto, L.; Caminero, F.; Cash, L.; Makris, C.; Lamichhane, P.; Deshmukh, R. R. Resistance to Checkpoint Inhibition in Cancer Immunotherapy. *Transl. Oncol.* **2020**, *13* (3), 100738.
- Zhou, B.; Gao, Y.; Zhang, P.; Chu, Q. Acquired Resistance to Immune Checkpoint Blockades: The Underlying Mechanisms and Potential Strategies. *Front. Immunol.* **2021**, *12*, 693609.
- Maruhashi, T.; Sugiura, D.; Okazaki, I.; Okazaki, T. LAG-3: from molecular functions to clinical applications. *J. Immunother. Cancer.* **2020**, *8* (2), No. e001014.
- Goldberg, M. V.; Drake, C. G. LAG-3 in Cancer Immunotherapy. *Curr. Top. Microbiol. Immunol.* **2010**, *344*, 269–278.
- Chocarro, L.; Blanco, E.; Arasan, H.; Fernandez-Rubio, L.; Bocanegra, A.; Echaide, M.; Garnica, M.; Ramos, P.; Fernandez-Hinojal, G.; Vera, R.; Kochan, G.; Escors, D. Clinical landscape of LAG-3-targeted therapy. *Immuno-Oncology Technol.* **2022**, *14*, 100079.
- Andrews, L. P.; Cillo, A. R.; Karapetyan, L.; Kirkwood, J. M.; Workman, C. J.; Vignali, D. Molecular Pathways and Mechanisms of LAG-3 in Cancer Therapy. *Clin. Cancer Res.* **2022**, *28* (23), 5030–5039.
- Triebel, F.; Jitsukawa, S.; Baixeras, E.; Roman-Roman, S.; Genevee, C.; Viegas-Pequignot, E.; Hercend, T. LAG-3, a novel lymphocyte activation gene closely related to CD4. *J. Exp. Med.* **1990**, *171*, 1393–405.
- Okazaki, T.; Okazaki, I.; Wang, J.; Sugiura, D.; Nakaki, F.; Yoshida, T.; Kato, Y.; Fagarasan, S.; Muramatsu, M.; Eto, T.; Hioki, K.; Honjo, T. PD-1 and LAG-3 inhibitory co-receptors act synergistically to prevent autoimmunity in mice. *J. Exp. Med.* **2011**, *208*, 395–407.
- Liang, B.; Workman, C.; Lee, J.; Chew, C.; Dale, B.; Colonna, L.; Flores, M.; Li, N.; Schweighoffer, E.; Greenberg, S.; Tybulewicz, V.; Vignali, D.; Clynes, R. Regulatory T cells inhibit dendritic cells by lymphocyte activation gene-3 engagement of MHC class II. *J. Immunol.* **2008**, *180* (9), 5916–5926.
- Andreae, S.; Buisson, S.; Triebel, F. MHC class II signal transduction in human dendritic cells induced by a natural ligand, the LAG-3 protein (CD223). *Blood* **2003**, *102* (6), 2130–2137.
- Wang, J.; Sanmamed, M. F.; Datar, I.; Su, T. T.; Ji, L.; Sun, J.; Chen, L.; Chen, Y.; Zhu, G.; Yin, W.; Zheng, L.; Zhou, T.; Badri, T.; Yao, S.; Zhu, S.; Boto, A.; Sznol, M.; Melero, I.; Vignali, D.; Schalper, K.; Chen, L. Fibrinogen-like protein 1 is a major immune inhibitory ligand of LAG-3. *Cell* **2019**, *176*, 334–347.
- Shi, A.-P.; Tang, X.-Y.; Xiong, Y.-L.; Zheng, K.-F.; Liu, Y.-J.; Shi, X.-G.; Lv, Y.; Jiang, T.; Ma, N.; Zhao, J.-B. Immune checkpoint

LAG3 and its ligand FGL1 in cancer. *Front. Immunol.* **2022**, *12*, 785091.

(20) Andrews, L. P.; Marciscano, A. E.; Drake, C. G.; Vignali, D. A. LAG3 (CD223) as a cancer immunotherapy target. *Immunol. Rev.* **2017**, *276* (1), 80–96.

(21) Andrews, L. P.; Yano, H.; Vignali, D. A. Inhibitory receptors and ligands beyond PD-1, PD-L1, and CTLA-4: breakthroughs or backups. *Nat. Immunol.* **2019**, *20* (11), 1425–1434.

(22) McLane, L. M.; Abdel-Hakeem, M. S.; Wherry, E. J. CD8 T cell exhaustion during chronic viral infection and cancer. *Annu. Rev. Immunol.* **2019**, *37*, 457–495.

(23) Turnis, M. E.; Andrews, L. P.; Vignali, D. A. Inhibitory receptors as targets for cancer immunotherapy. *Eur. J. Immunol.* **2015**, *45* (7), 1892–1905.

(24) Matsuzaki, J.; Gnjatic, S.; Mhawech-Fauceglia, P.; Beck, A.; Miller, A.; Tsuji, T.; Eppolito, C.; Qian, F.; Lele, S.; Shrikant, P.; Old, L.; Odunsi, K. Tumor-infiltrating NY-ESO-1-specific CD8+ T cells are negatively regulated by LAG-3 and PD-1 in human ovarian cancer. *Proc. Natl. Acad. Sci. U.S.A.* **2010**, *107* (17), 7875–7880.

(25) Woo, S. R.; Turnis, M. E.; Goldberg, M. V.; Bankoti, J.; Selby, M.; Nirschl, C.; Bettini, M.; Gravano, D.; Vogel, P.; Liu, C.; Tangsombatvisit, S.; Grosso, J.; Netto, G.; Smeltzer, M.; Chaux, A.; Utz, P.; Workman, C.; Pardoll, D.; Korman, A.; Drake, C.; Vignali, D. Immune inhibitory molecules LAG-3 and PD-1 synergistically regulate T-cell function to promote tumoral immune escape. *Cancer Res.* **2012**, *72* (4), 917–927.

(26) Chen, J.; Chen, Z. The effect of immune microenvironment on the progression and prognosis of colorectal cancer. *Med. Oncol.* **2014**, *31* (8), 82.

(27) FDA approves anti-LAG3 checkpoint. *Nat. Biotechnol.* **2022**, *40* (5), 625.

(28) Lee, C. M.; Tannock, I. F. The distribution of the therapeutic monoclonal antibodies cetuximab and trastuzumab within solid tumors. *BMC Cancer* **2010**, *10* (1), 255.

(29) Scott, A. M.; Wolchok, J. D.; Old, L. J. Antibody therapy of cancer. *Nat. Rev. Cancer* **2012**, *12* (4), 278–287.

(30) Imai, K.; Takaoka, A. Comparing antibody and small-molecule therapies for cancer. *Nat. Rev. Cancer* **2006**, *6* (9), 714–727.

(31) Hernandez, I.; Bott, S. W.; Patel, A. S.; Wolf, C. G.; Hospodar, A. R.; Sampathkumar, S.; Shrank, W. H. Pricing of monoclonal antibody therapies: higher if used for cancer? *Am. J. Manag. Care.* **2018**, *24* (2), 109–112.

(32) Centanni, M.; Moes, D. J.; Trocóniz, I. F.; Ciccolini, J.; van Hasselt, J. G. Clinical Pharmacokinetics and Pharmacodynamics of Immune Checkpoint Inhibitors. *Clin. Pharmacokinet.* **2019**, *58* (7), 835–857.

(33) Sosa, A.; Cadena, E.; Olive, C.; Karachaliou, N.; Rosell, R. Clinical assessment of immune-related adverse events. *Ther. Adv. Med. Oncol.* **2018**, *10*, 175883591876462.

(34) Ryman, J. T.; Meibohm, B. Pharmacokinetics of Monoclonal Antibodies. *CPT Pharmacometrics Syst. Pharmacol.* **2017**, *6* (9), 576–588.

(35) Kerr, W.; Chisholm, J. The next generation of immunotherapy for cancer: Small molecules could make big waves. *J. Immunol.* **2019**, *202*, 11–19.

(36) Gabr, M. T.; Gambhir, S. S. Discovery and Optimization of Small-Molecule Ligands for V-Domain Ig Suppressor of T-Cell Activation (VISTA). *J. Am. Chem. Soc.* **2020**, *142* (38), 16194–16198.

(37) Maruhashi, T.; Sugiura, D.; Okazaki, I. M.; Shimizu, K.; Maeda, T. K.; Ikubo, J.; Yoshikawa, H.; Maenaka, K.; Ishimaru, N.; Kosako, H.; Takemoto, T.; Okazaki, T. Binding of LAG-3 to stable peptide-MHC class II limits T cell function and suppresses autoimmunity and anti-cancer immunity. *Immunity.* **2022**, *55* (5), 912–924.

(38) Thudium, K.; Selby, M.; Zorn, J. A.; Rak, G.; Wang, X.-Z.; Bunch, R.-T.; Hogan, J.; Strop, P.; Korman, A. J. Preclinical characterization of relatlimab, a human LAG-3-blocking antibody, alone or in combination with nivolumab. *Cancer Immunol. Res.* **2022**, *10* (10), 1175–1189.

(39) Lipinski, C. A.; Lombardo, F.; Dominy, B. W.; Feeney, P. J. Experimental and computational approaches to estimate solubility and permeability in drug discovery and development settings. *Adv. Drug Delivery Rev.* **1997**, *23* (1), 3–25.

(40) Baell, J. B.; Holloway, G. A. New substructure filters for removal of pan assay interference compounds (PAINS) from screening libraries and for their exclusion in bioassays. *J. Med. Chem.* **2010**, *53* (7), 2719–2740.

(41) Hall, R. J.; Murray, C. W.; Verdonk, M. L. The fragment network: A chemistry recommendation engine built using a graph database. *J. Med. Chem.* **2017**, *60* (14), 6440–6450.

(42) Borysko, P.; Moroz, Y.; Vasylenko, O. V.; Hurmach, V. V.; Starodubtseva, A.; Stefanishena, N.; Nesteruk, K.; Zozulya, S.; Kondratov, I. S.; Grygorenko, O. Straightforward hit identification approach in fragment-based discovery of bromodomain-containing protein 4 (BRD4) inhibitors. *Bioorg. Med. Chem.* **2018**, *26* (12), 3399–3405.

(43) Sijbesma, E.; Visser, E.; Plitzko; Thiel, P.; Milroy, L.-G.; Kaiser, M.; Brunsveld, L.; Ottmann, C. Structure-based evolution of a promiscuous inhibitor to a selective stabilizer of protein-protein interactions. *Nat. Commun.* **2020**, *11*, 3954.